Underwater Robotic: localization with electrolocation for collision avoidance

G. Baffet, Pol-Bernard Gossiaux, Mathieu Porez, Frédéric Boyer

Underwater Robotic: localization with electrolocation for collision avoidance

Guillaume Baffet, Pol Bernard Gossiaux, Mathieu Porez and Frédéric Boyer

***Abstract*— This paper proposes and compares two observers designed to calculate the location of an obstacle. The two methods are bio-inspired with a sense used by electric fishes of equatorial forests: *the electrolocation*. Firstly, this study presents the electrolocation and then develops two models of emitter-sensors inspired by the electrical sense. Secondly, the two models are used in different observers for detection and localisation of wall obstacles. The estimation methods are based on an Extended Kalman Filter algorithm. Observers are tested on simulations in order to assess their potentials and to analyze observability.**

I. INTRODUCTION

The perception of aquatic surroundings is essential for the enhancement of safety and trajectory-control systems of underwater robots. There are various applications such as recognition, object location and obstacle avoidance. This study focuses on the perception in troubled and dark waters. In these conditions, classical approaches based on sound and optics, *i.e. sonars and cameras*, are nowadays inadequate. The perception method applied here is bio-inspired from the electric sense *electrolocation* discovered recently in the 50*s* by H.W. Lissman [9]. This sense is employed by electric fishes in order to explore, hunt and communicate in dark and muddy environments [10], [16], [17].

For electric fishes, the principle of active electrolocation is based on electric field emissions produced by an *Electric Organ Discharge* (EOD, illustrated in Fig. 1). The field lines are focalized by the fish body because of its height conductivity. Disseminated in the skin, numerous fish sensors gather electric information, then the fish has an *electric image* of it surroundings. In the presence of obstacles, the electric field is distorted in such a way that the fish deduces caracteristics (distance, dimension, geometry, conductivity, ..) of the obstacle.

Electrolocation has been widely discussed in biology, neuroscience literature [3], [5], [6], however this reseach domain has stayed open in robotics and mechatronics. In [14], B. Rasnow presents a theoretical model of electric deformation induced by an obstacle with spherical shape. This model is used by J. Solberg in [15] with an eye to locate *spherical objects*. The sphere location is estimated according to the measurements of an electrical emitter-sensor. This sensor is placed on a *mobile stand which moves step-by-step*. The main differences in this present study, are the obstacle to locate has an *infinite wall shape*, and the emitter-sensor is settled on a *mobile fish robot*.

This study is realized in the RAAMO project, the continuation of a ROBEA project[1], where the main results are experimental bench development (Fig. 2), modeling and feedback laws for the 3D movement of an Eel-like robot [1], [4]. Following the biomimetic path, our objective is to endow the Eel-like robot of a mecatronic system reproducing the electrolocation sense, in order to locate the object for collision avoidance. With a view to accomplish this objective, this study develops and compares two different observers, represented in Fig. 3, denoted $O_{fk,1}$ and $O_{fk,2}$. These estimators require in entry the measurements of robot dynamic and electric sensing. They are constructed according

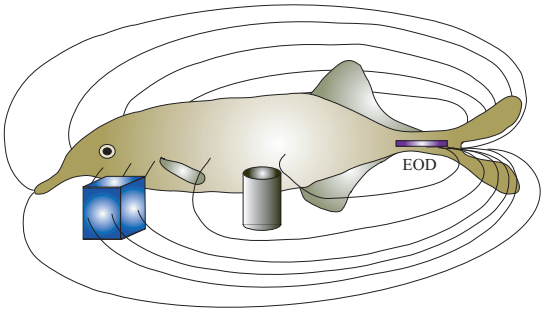

Fig. 1. Electric fish, field distorted by two obstacles. The cylinder represents an insulator, field lines are deviated whereas the cube is a conductor, focalizing electric field.

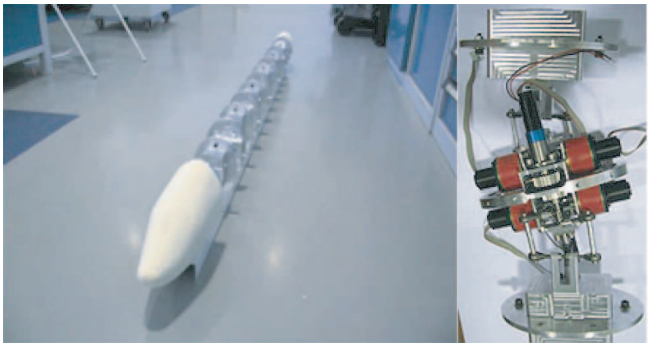

Fig. 2. Experimental bench: on the left, Eel-like robot, on the right, a robot vertebra.

This work was supported by ANR (Agence nationale de la recherche)

G. Baffet, P.B. Gossiaux, M. Porez and F. Boyer are with Ecole des Mines de Nantes, La Chantrerie, Nantes, France

G. Baffet, M. Porez and F. Boyer are with the IRCCyN Laboratory, UMR CNRS 6597, guillaume.baffet@emn.fr, mathieu.porez@emn.fr, frederic.boyer@emn.fr

P.B. Gossiaux is with the SUBATECH Laboratory, UMR CNRS 6457, gossiaux@emn.fr

[1]RAAMO: Robot Anguille Autonome pour Milieux Opaques, 2007-2010, ROBEA: Robotique et Entités Artificielles, Eel-robot, 2004-2007

to the same locomotion model and are different in their emitter-sensor models: *2-spheres* and *4-hemispheres*. These models are applied in extended Kalman Filters to calculate the position and orientation of an infinite wall obstacle.

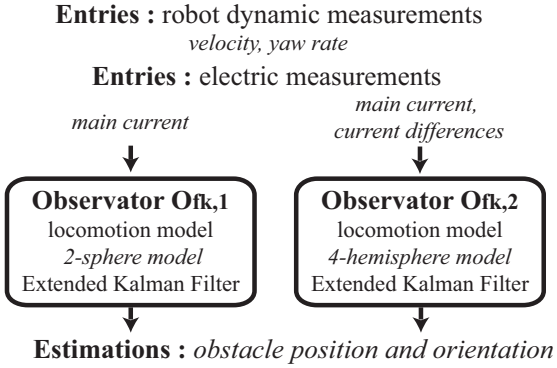

Fig. 3. Locating processes, observators $O_{fk,1}$ and $O_{fk,2}$

A. Paper organization

The next section proposes two emitter-sensor models and a simplified locomotion model. The second part presents the estimation process, definitions and tools for the observability analysis. The last part of the paper describes the observer evaluation in simulations. Table I lists the different notations.

TABLE I
NOMENCLATURE

Symbol	Description
d	Distance between robot and wall
α	Angle between robot and wall
e	Emitter-sensor tension
I	Emitter-sensor main current
$I_{f,l}$, $I_{f,r}$	Front, left, right current
$I_{r,l}$, $I_{r,r}$	Rear, left, right current
γ	Conductivity
ε	Permittivity
Γ_{env}	Conductance "water and obstacle"
L	Distance between spheres
R	Sphere radius
Q	Charge Quantity
V_t, V_q	Front and rear potentials
$\mathbf{X}, \mathbf{U}, \mathbf{Y}$	State, entry, measurement vectors
$\mathbf{f}$, $\mathbf{g}$	Evolution, measurement functions

II. ROBOT-ELECTROLOCATION-OBSTACLE MODELING

The final mecatronic system will be composed of numerous sensors in the Eel-like robot skin. However, preliminary of the development of the whole mecatronic system (with its all complexity), the system is analysed in two simple forms: 2-spheres and 4-hemispheres.

A. First emittor-sensor model: 2-spheres

Represented in Fig. 4, the emitter-sensor is modeled with a dipolar comprising two spheres of radius R, separated with a distance $L \gg R$. A tension e induces opposite charge quantities in the spheres ($+Q$ and $-Q$). Current density is created in the aquatic surroundings between the two spheres. The total electric current I, along with charge quantities $\pm Q$, depends on environment resistivity and so the obstacle presence.

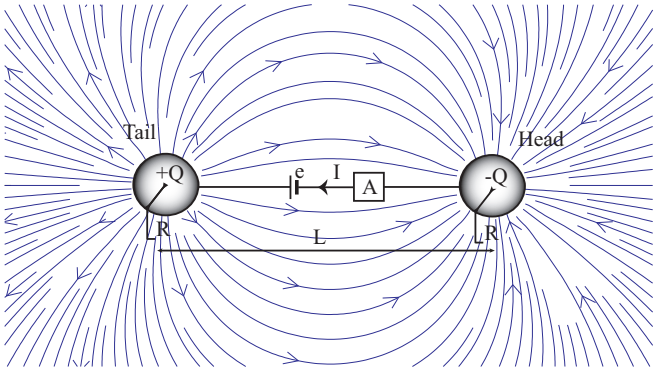

Fig. 4. 2-spheres Model of the electric emittor-sensor.

1) Current intensity I in wall presence: The wall position relative to the robot is represented with distance d and angle α (see Fig. 5). The wall is assumed insulating. In this assumption, the electric current field stays clear from the wall and is parallel in its proximity. The wall interacts with the dipole like another dipole in location $-d$, $\pi - \alpha$ (illustrated in Fig. 5), and so the current I is calculated using the method of image [7].

Consider ε is the environnement permittivity, d_t and d_q are geometric variables. Electric potentials at the spheres, V_t and

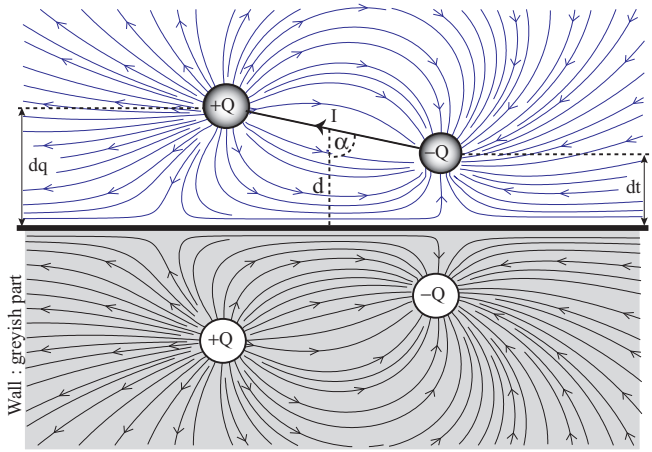

Fig. 5. System in the presence of a wall obstacle. Illustration of the dipole reflection.

V_q, are the sums of the potential impacts originally from the four spheres:

$$V_t \approx -\frac{Q}{4\pi\varepsilon}\left[\frac{1}{R}-\frac{1}{L}+\frac{1}{2d_t}-\frac{1}{\sqrt{4d_td_q+L^2}}\right],$$
$$V_q \approx \frac{Q}{4\pi\varepsilon}\left[\frac{1}{R}-\frac{1}{L}+\frac{1}{2d_q}-\frac{1}{\sqrt{4d_td_q+L^2}}\right], \quad (1)$$

mutual polarisation being neglected because it is assumed that $L, d_t, d_q \gg R$. The potential difference $V_t - V_q$ is equal

to tension e:

$$\begin{aligned} e &\approx V_t - V_q, \\ e &\approx \frac{Q}{4\pi\varepsilon}\left[\frac{2}{R} - \frac{2}{L} + \frac{1}{2d_q} + \frac{1}{2d_t} - \frac{2}{\sqrt{4d_t d_q + L^2}}\right], \end{aligned} \tag{2}$$

so charge quantity Q is formulated as the following relationship:

$$Q \approx 2\pi\varepsilon R\left[\left(1+\frac{R}{L}\right) - R\left(\frac{d_t+d_q}{4d_t d_q} - \frac{1}{\sqrt{4d_t d_q + L^2}}\right)\right]e. \tag{3}$$

The total current I crossing over each sphere, entering by the robot head, leaving by the tail, is calculated applying the integral theorem of gauss:

$$I = \Phi_{S_q}(\overrightarrow{j}) = \gamma\Phi_{S_q}(\overrightarrow{E}) = \frac{\gamma}{\varepsilon}Q, \tag{4}$$

where $\Phi_S(\overrightarrow{Z})$ is defined as the flow of a field $\overrightarrow{Z}$, on the closed surface S. The variable S_q represents a closed surface around the head sphere, $\overrightarrow{j}$ is the current density, $\overrightarrow{E}$ is the electric field, and γ is the environment conductivity. The current formulation is:

$$I \approx \Gamma_{env} e, \tag{5}$$

where Γ_{env} is the conductivity of the surroundings (obstacle and water):

$$\Gamma_{env} = \gamma 2\pi R[\left(1+\frac{R}{L}\right) - R(\frac{2d}{4d^2 - L^2\cos^2(\alpha)} - \frac{1}{\sqrt{4d^2 + L^2\sin^2(\alpha)}})]. \tag{6}$$

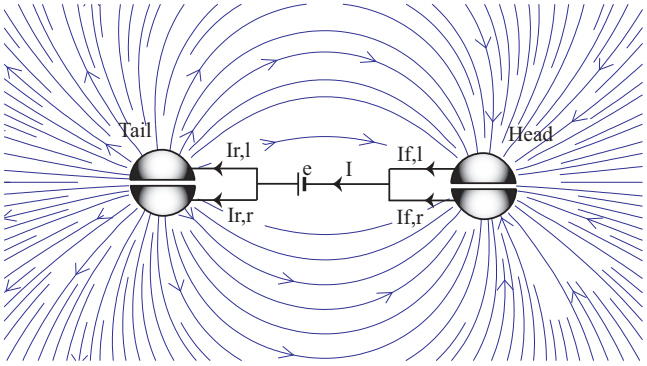

Fig. 6. 4-hemispheres model of the electric emittor-sensor.

B. Second emittor-sensor model: 4-hemispheres

As shown in Fig. 6, the head and tail are now constructed with hemispheres. Consider $I_{f,l}$ (respectively $I_{f,r}$) the current coming by left hemisphere (respectively right) of the head, and $I_{r,l}$, $I_{r,r}$ currents leaving by the tail. In the absence of disturbances, currents satisfy the equalities $I_{f,l} = I_{f,r} = I_{r,l} = I_{r,r} = I/2$, for symetric reasons. The idea is that the presence of an obstacle on the right or on the left will change this symetry and so the comparison between left and right currents reproduce an stereoscopic electrolocation. Differences between right and left currents are calculated as:

$$\begin{aligned} I_{f,r} - I_{f,l} &\approx -3\gamma R^3\pi e\sin(\alpha)[\frac{1}{(2d - L\cos(\alpha))^2} \\ &- \frac{2d + L\cos(\alpha)}{(4d^2 + L^2\sin^2(\alpha))^{3/2}}], \\ I_{r,r} - I_{r,l} &\approx -3\gamma R^3\pi e\sin(\alpha)[\frac{1}{(2d + L\cos(\alpha))^2} \\ &- \frac{2d - L\cos(\alpha)}{(4d^2 + L^2\sin^2(\alpha))^{3/2}}] \end{aligned} \tag{7}$$

C. Robot locomotion modeling

A main objective of this study is the observability evaluation of measurement systems. In this view, the model describes electrolocation and reduces locomotion representation. The evolution model represents a dipole sailing with a velocity V, and a yaw rate $\dot{\psi}$ (illustrated in Fig. 7). Simplified dynamic equations of (d, α) are the following:

$$\begin{aligned} \dot{d} &= -V\cos(\alpha), \\ \dot{\alpha} &= \dot{\psi}. \end{aligned} \tag{8}$$

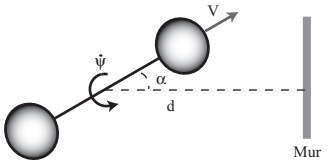

Fig. 7. Simplified locomotion model of the Eel-like robot.

III. Estimators $O_{fk,1}$, $O_{fk,2}$ and observability

A. Models of the two systems

Systems $O_{fk,1}$ and $O_{fk,2}$ have same components in their state vector $\mathbf{X}$ and entry vector $\mathbf{U}$:

$$\begin{aligned} \mathbf{U} &= [V, \dot{\psi}]^\top = [u_1, u_2]^\top, \\ \mathbf{X} &= [d, \alpha]^\top = [x_1, x_2]^\top. \end{aligned} \tag{9}$$

Likewise, their evolution models are equivalents:

$$\dot{\mathbf{X}} = \mathbf{f}(\mathbf{X}, \mathbf{U}) = \left[\ -u_1\cos(x_2), u_2\ \right]^\top, \tag{10}$$

where $\mathbf{f}$ is the evolution function. The two observers are different in their measurement vectors $\mathbf{Y}$ and models $\mathbf{g}$:

- for $O_{fk,1}$:

$$\begin{aligned} \mathbf{Y} &= \mathbf{g}(\mathbf{X}, \mathbf{U}) = I, \\ \mathbf{Y} &= \left[\begin{array}{c} 2\pi R\gamma e[\left(1+\frac{R}{L}\right) - R(\frac{2x_1}{4x_1^2 - L^2\cos^2(x_2)} \\ -\frac{1}{\sqrt{4x_1^2 + L^2\sin^2(x_2)}})] \end{array}\right], \end{aligned} \tag{11}$$

- for $O_{fk,2}$:

$$\mathbf{Y} = \mathbf{g}(\mathbf{X},\mathbf{U}) = [I, I_{f,r} - I_{f,l}, I_{r,r} - I_{r,l}],$$

$$\mathbf{Y} = \begin{bmatrix} 2\pi R\gamma e[\left(1+\frac{R}{L}\right) - R(\frac{2x_1}{4x_1^2 - L^2\cos^2(x_2)} \\ \quad - \frac{1}{\sqrt{4x_1^2 + L^2\sin^2(x_2)}})], \\ -3\gamma R^3 \pi e \sin(x_2)[\frac{1}{(2x_1 - L\cos(x_2))^2} \\ \quad - \frac{2x_1 + L\cos(x_2)}{(4x_1^2 + L^2\sin^2(x_2))^{3/2}}], \\ -3\gamma R^3 \pi e \sin(x_2)[\frac{1}{(2x_1 + L\cos(x_2))^2} \\ \quad - \frac{2x_1 - L\cos(x_2)}{(4x_1^2 + L^2\sin^2(x_2))^{3/2}}], \end{bmatrix}, \quad (12)$$

Observers $O_{fk,1}$ and $O_{fk,2}$ are based on an extended Kalman filter algorithm [8], [11], [2].

B. Obstacle detection

When the sensor gets away from the wall, current measurement I decreases quickly and the wall becomes rapidly "invisible". In these conditions, observers cannot estimate accurately the wall location, as a consequence state estimates can diverge. For this reason, observers are "set in motion" only when the robot is near an obstacle, that is when measured current I is sufficiently disturbed to infer the obstacle presence.

C. Local observability

This section presents an observability method and definitions [12], which are used in section IV in order to analyse and to justify results.

Definition 1: Two states $\mathbf{X_1}$, $\mathbf{X_2}$ are said to be *indistinguishable* (denoted $\mathbf{X_1 I X_2}$) if for every admissible input function $\mathbf{U}$, the output function $\mathbf{Y}(t, \mathbf{X_1}, \mathbf{U})$, $t \geq 0$, of the system for the initial state $\mathbf{X}(0) = \mathbf{X_1}$, and the output function $\mathbf{Y}(t, \mathbf{X_2}, \mathbf{U})$, $t \geq 0$, of the system for the initial state $\mathbf{X}(0) = \mathbf{X_2}$, are equal. The system is called *observable* if $\mathbf{X_1 I X_2}$ implies $\mathbf{X_1} = \mathbf{X_2}$.

Definition 2: The system is called *locally observable* at $\mathbf{X_1}$, if there is a neighborhood $\mathbf{W}$ of $\mathbf{X_1}$ such that for every neighborhood $\mathbf{X_2} \subset \mathbf{W}$ the relation $\mathbf{X_1 I X_2}$ implies $\mathbf{X_1} = \mathbf{X_2}$.

The model is non-linear, so observability is analyzed locally, around a state and an entry [12]. An observability matrix is calculated according to Lie derivative, and the state is called locally observable if the rank of this matrix is equal to the state dimension.

IV. Evaluation in simulation

Observers $O_{fk,1}$ and $O_{fk,2}$ are compared using data obtained in simulation. Among numerous tests, three robot approaches toward the wall are presented: *in slalom*, *in full-face* and *in diagonal*. Fish-robot paths for the three tests are presented in Fig. 8. During the first test (slalom), the robot comes close to the wall, then runs parallel to it undergoing a slalom. The yaw rate is not null in the major part of this test. At the second test, the robot swims toward the wall with an angle $\alpha = 0$ and a yaw rate equal to zero. At the third and latest test, the robot approaches the obstacle in a diagonal without a yaw rate and with an angle approximately at 80^o. As regards conductivity setting, it represents a pure water

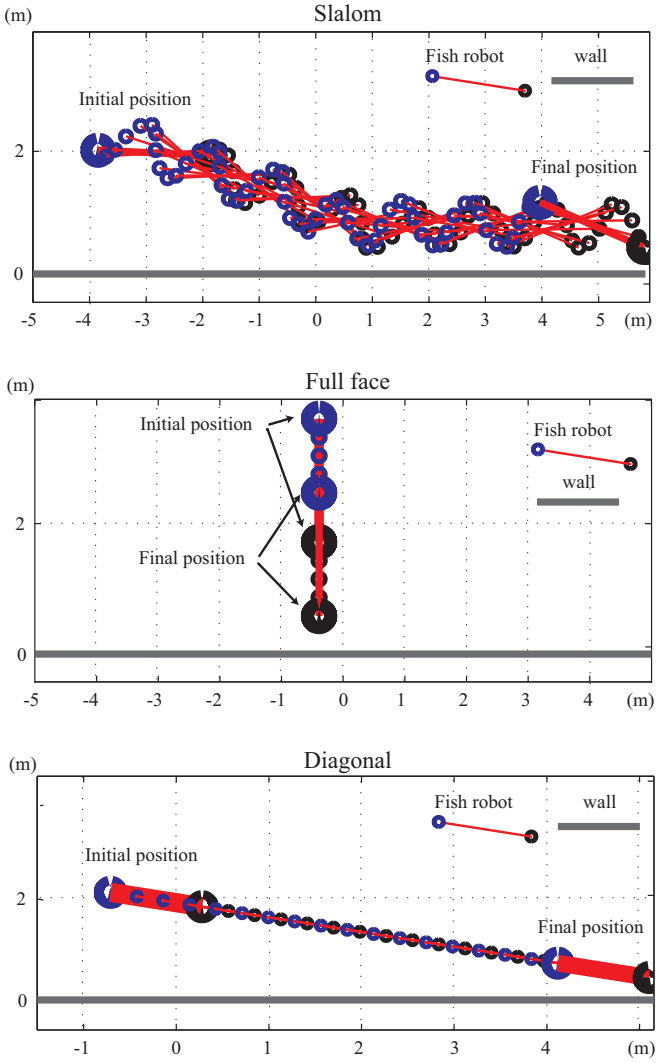

Fig. 8. Robot paths for the three simulation tests. Initial and final robot positions are traced out thickly.

with a weak conductance, about 0.01 S/m. Robot velocity V stays constant whatever the test, and equal to 1 m/s. It is an unfavorable case because the intended velocity of the robot is inferior (about 0.5 m/s).

Fig. 9 presents estimation results of wall distance d and orientation α, obtained from $O_{fk,1}$ and $O_{fk,2}$ observers for the first test (slalom). Up to the fourth second, the robot is not sufficiently close to the wall to detect the obstacle, consequently observer estimations remain at their

TABLE II

Convergence time and wall distances.

Test	Observer	Time (s)	Distance (m)
1er test, Slalom	$O_{fk,1}$	5	0.8
	$\mathbf{O_{fk,2}}$	**0.3**	**1.4**
2nd test, ($\perp$ wall)	$O_{fk,1}$	0.1	2
	$\mathbf{O_{fk,2}}$	**0.1**	**2**
3rd test, 80^0/wall	$O_{fk,1}$	8	0.65
	$\mathbf{O_{fk,2}}$	**1.1**	**1.3**

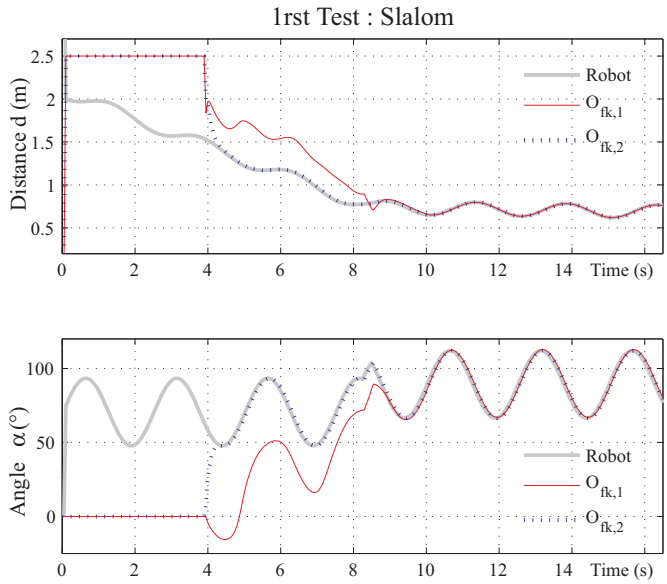

Fig. 9. Slalom test. Observers $O_{fk,1}$ and $O_{fk,2}$. Estimation results of wall position d and angle α.

initial values. From $t = 4$ s, electric current variations are sufficiently important, the wall is detected, so observers $O_{fk,1}$ and $O_{fk,2}$ are "set in motion". Estimation convergences are significantly different according to the used observer. In fact, estimations from observer $O_{fk,2}$ are faster than the ones of $O_{fk,1}$. This can be explained because observer $O_{fk,2}$ uses more information (measurements) than observer $O_{fk,1}$. Table II presents convergence times and associated wall distance d. This table confirms the fastness of $O_{fk,2}$ (0.3 s) comparatively to $O_{fk,1}$ (5 s) and shows the distance where the location estimations are relatively accurate.

Transfered in Fig. 10, results show in the second test that

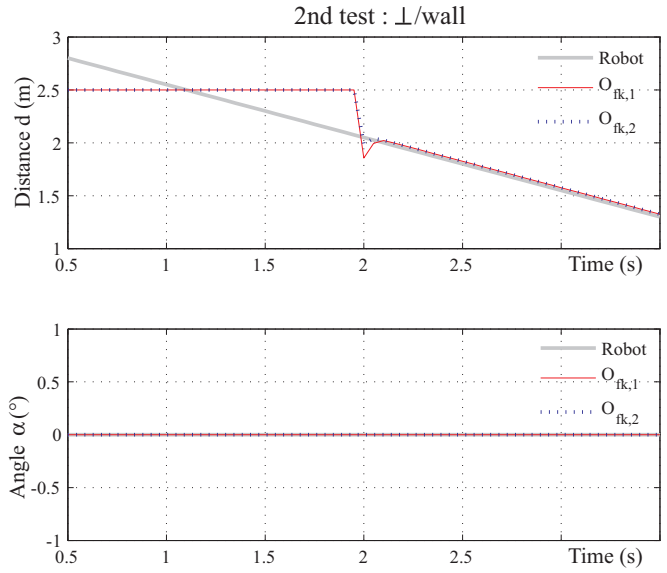

Fig. 10. Second test ⊥/wall. Observers $O_{fk,1}$ and $O_{fk,2}$. Estimation results of wall position d and angle α.

the two observers provide similar estimations close to the measurements. The obstacle is detected approximately at $t \simeq 2$ s, and is located in a time of 0.1 s and with a wall distance of 2 meters.

Fig. 11 retraces estimation results for the third test. In order to give prominence to observability results, estimates were initialized at two different values:

- initialization 1, $[d = 2.5m, \alpha = 0.1rad]$, and
- initialization 2, $[d = 2.5m, \alpha = -0.1rad]$.

The obstacle is detected at $t = 8.3$ s, then the convergences become significantly different according to the distance d or the angle α.

- As regard distance estimates, this test corroborates the results of the first test, that is the fastest convergence of $O_{fk,2}$ estimates.
- For angle α estimates, observer $O_{fk,2}$ gives satisfactory and good results whatever the two initializations. This is not the case for $O_{fk,1}$ observer. Indeed, when α estimate is initialized at 0.1 radians, it converges toward the true value $\alpha \simeq 1.4$ radians, whereas for an initialization at -0.1 radians, it converges towards the false value $\alpha \simeq -1.4$ radians. These different results are explained hereinafter in the observability analysis.

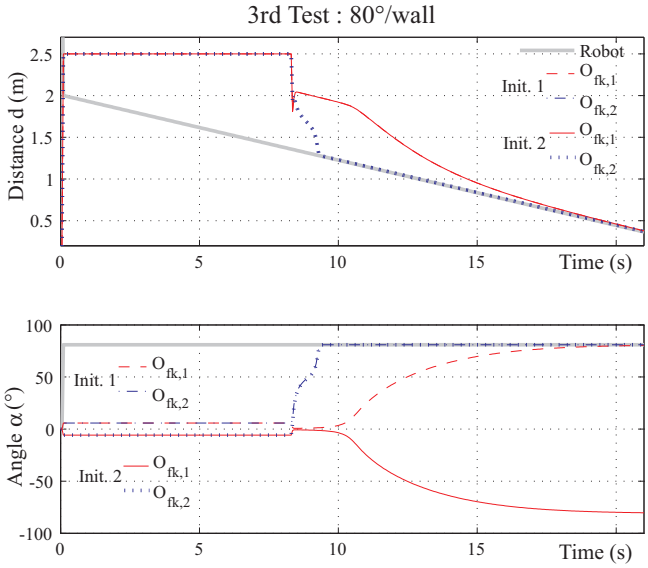

Fig. 11. Third test 80^0/wall. Observers $O_{fk,1}$ and $O_{fk,2}$. Estimation results of wall position d and angle α.

A. Observability analysis

Ranks of observability matrix associated to $O_{fk,1}$ and $O_{fk,2}$ were calculated at each time steps for the three tests. At the first test, the observability matrix remains at a rank of two, so the system is locally observable, tacitly confirmed by the relatively good estimates.

In the second test, yaw rate $\dot{\psi}$ and angle α are null, then ensue different observability ranks, with a rank of 2 for $O_{fk,2}$ model, which is locally observable, and a rank of 1 for $O_{fk,1}$ model, which is not observable. In fact, when:

- $\alpha = 0,\ \psi = 0,\ d = d_1,\ V = V_1,\ \forall d_1,\ \forall V_1,$

the neighbours dissent from a small ξ, such as

- $X_1 = [d_1, \alpha = +\xi/2]$ and
- $X_2 = [d_1, \alpha = -\xi/2]$, (see Fig. 12),

are indistinguishable because measurements I are the same in the two cases. So the system $O_{fk,1}$ is not locally observable (definition 2 in section III-C). If the system $O_{fk,1}$ would be improved with measurements ($I_{f,r} - I_{f,l}$, $I_{r,r} - I_{r,l}$), it would become observable (case $O_{fk,2}$, *stereoscopy*).

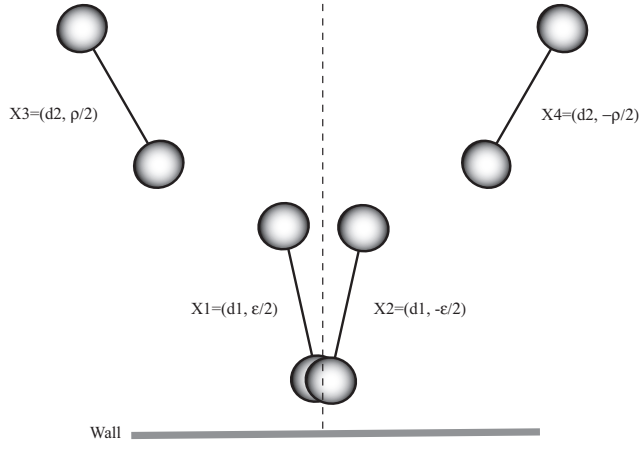

Fig. 12. Indistinguishable cases. Yaw rate is null, V velocity is the same, state X_1 is indistinguishable with X_2, and X_3 is indistinguishable with X_4.

At the third test, observability ranks are equal to 2, so states of the two systems are locally observable. However, the state of the first system $O_{fk,1}$ is not observable. Indeed, around the state:

- $\alpha = \rho/2,\ \psi = 0,\ d = d_2,\ V = V_2,\ \forall d_2,\ \forall V_2,\ \|\rho\| > 0,$

the closed neighbours are indistinguishable (conferring the local observability), however the two states:

- $X_3 = [d_2, \alpha = \rho/2]$,
- $X_4 = [d_2, \alpha = -\rho/2]$, (see Fig. 12)

are indistinguishable, so not observable. As a consequence, the estimate convergence towards one or the other of these indistinguishable states is strongly conditional on the initialization. This is shown in the third test for the angle α estimates of observer $O_{fk,1}$ (Fig 11). In one case, the estimation converges toward $\alpha = 80^0$ whereas in the other case, it converges toward its opposite $\alpha = -80^0$.

V. Conclusion

This study proposes two observers, $O_{fk,1}$ and $O_{fk,2}$, for the location of a wall obstacle. They are based on electrolocation and different emittor-sensor models: 2-spheres and 4-hemispheres. Simulation results show that the first observer $O_{fk,1}$ provides satisfactory estimates if the state is well initialized because this system is only locally observable. The first observer is not sufficient because a "good initialization" is a priori not expectable. This justifies that the system complexity is increased by taking account of other measurements, notably electric current differences. That is done with the second observer $O_{fk,2}$, constructed with the emittor-sensor model 4-hemispheres. This observer gives obstacle location relative accuracy, whatever the test initializations, and improves the observability of the perception system using electrolocation.

A. Future Works

An emittor-sensor based on the "2-spheres" model is under construction and it will be placed in an experimental aquarium bench. Then, future works will evaluate experimentally the physical model "2-spheres", the observability analysis, and the observers.

VI. Acknowledgments

We thank Kirsty Grant for helpful discussions regarding the field of electric fishes. We are grateful to Noel Servagent and Stephane Bouvier for their role in the development of the emittor-sensor.

References

[1] M. Alamir, G. Hafidi, N. Marchand, M. ElRafei, M. Porez and F. Boyer. *Feedback Design for 3D Movement of an Eel like Robot*, Proceedings of the IEEE Conference on Robotics and Automation, Roma, Italy, 2007.

[2] G. Baffet, A. Charara and G. Dherbomez. *An observer of tire-road forces and friction for active-security vehicle systems*, IEEE Mechatronics, 12(6), December, 2007.

[3] C. Bell, V. Han, Y. Sugawara, and K. Grant. *Plasticity in the mormyrid electrosensory lobe*, J. Exp. Biology, 202: 1339-1347, 1999.

[4] F. Boyer, M. Porez and W. Khalil, *Macro-continuous computed torque algorithm for a three-dimensional eel-like robot*, IEEE Transactions on Robotics, 22(4):763-775, 2006.

[5] A. Caputi, R. Budelli, K. Grant, and C.C. Bell. *The electric image in weakly electric fish: II. Physical images of resistive objects in Gnathonemus petersii*, Journal of Experimental Biology, 201: 2115-2128, 1998.

[6] K. Grant, G. von der Emde, L. Gomez-Sena and C. Mohr. *Neural command of electromotor output in mormyrids*, Journal of Experimental Biology. 202: 1399-1407, 1999.

[7] J.D. Jackson. Classical Electrodynamics (2nd Edition). Wiley and Sons, 1975.

[8] R.E. Kalman. *A New Approach to Linear Filtering and Prediction Problems*, Transactions of the ASME - Journal of Basic Engineering, 82(d):35-45, 1960.

[9] H. W. Lissmann and K. E. Machin. *The mechanism of object location in Gymnarchus niloticus and similar fish*, J. Exp. Biol., 35:451-486, 1958.

[10] M.A. MacIver, N.M. Sharabash, M.E. Nelson. *Prey-capture behavior in gymnotid electric fish: motion analysis and effects of water conductivity*, Journal of Experimental Biology 204(3):543-557, 2001.

[11] S.G. Mohinder and P.A. Angus. *Kalman filtering theory and practice*, Prentice hall, 1993.

[12] H. Nijmeijer and A.J. Van der Schaft. *Nonlinear Dynamical Control Systems*, Springer-Verlag, 1990.

[13] M. Porez. *Modèle dynamique analytique de la nage tridimensionnelle anguilliforme pour la robotique*, thse, IRCCyN CNRS, cole des Mines de Nantes et Universit de Nantes, France, Septembre 2007.

[14] B. Rasnow. *The effects of simple objects on the electric field of Apteronotus*, J. Comp. Physiol. A, 178(3):397-411, 1996.

[15] J.R. Solberg, K.M. Lynch, and M.A. MacIver. *Robotic Electrolocation: Active Underwater Object Localization with Electric Fields*, in IEEE International Conference on Robotics and Automation. Rome, Italy, 2007.

[16] P.K. Stoddard, H.H. Zakon, M.R. Markham and L. McAnelly. *Regulation and modulation of electric waveforms in gymnotiform electric fish*, J Comp Physiol A, 192(6):613-24, 2006.

[17] G. von der Emde, S. Schwarz, L. Gomez-Sena, R. Budelli and K. Grant. *Electric fish measure distance in the dark*, Nature, 395:890-894, 1998.